Computational Methods for Design and Control of MEMS Micromanipulator Arrays

KARL F. BÖHRINGER, BRUCE R. DONALD, AND NOEL C. MACDONALD
Cornell University
GREGORY T.A. KOVACS AND JOHN W. SUH
Stanford University

◆   ◆   ◆

Arrays of MEMS devices can move and position tiny parts, such as integrated circuit chips, in flexible and predictable ways by oscillatory or ciliary action. The theory of programmable force fields can model this action, leading to algorithms for various types of micromanipulation that require no sensing of where the part is. Experiments support the theory.

◆

As improvements in fabrication technology for microelectromechanical systems, or MEMS, increase the availability and diversity of these micromachines, engineers are defining a growing number of tasks to which they can be put. The idea of carrying out tasks using large coordinated groups of MEMS units motivates the development of automated, algorithmic methods for designing and controlling these groups of devices. We report here on progress towards *computational MEMS*, taking on the challenge of design and control of massively parallel arrays of microactuators.

Programmable vector fields for MEMS control

Many industrial and other processes—for instance, integrated circuit manufacturing—require moving, positioning, and otherwise manipulating miriad tiny parts. This would seem to be a suitable task for MEMS devices if they could be controlled to act as miniature conveyor belts, robots, and so forth. Our goal is to implement task-level, sensorless manipulation strategies with arrays of microfabricated actuators. These tasks can be modeled by the *theory of programmable vector fields*,[1] first applied to micromanipulation in 1994,[2] which describes the forces generated by the actuators as planar vector fields. Recent results of our experiments with two different types of MEMS microactuator arrays are consistent with the behavior predicted by the theory of programmable force fields.

Abstraction barrier increases generality

This theory arguably represents the first systematic attack on massively parallel, distributed manipulation based on geometric and physical reasoning. Applications such as parts-feeding can be formulated in terms of the force vector fields required. Thus programmable force fields act as an *abstraction barrier* between applications requiring array micromanipulation and their implementation with MEMS devices. Such abstraction barriers permit hierarchical design, and allow application designs with greater independence from underlying device technology.

Given a task (such as uniquely positioning a part) and a part geometry, we develop algorithms that automatically generate the corresponding manipulation plans as a sequence of force fields. We also derive a classification of vector fields, resulting in design criteria by which efficient
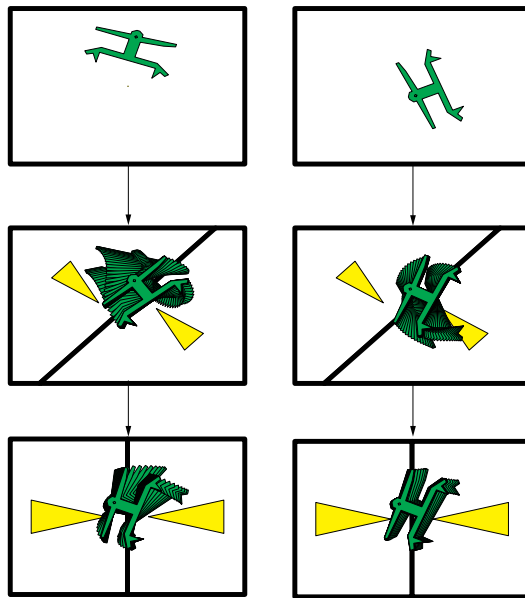
Figure 1. Sensorless parts orienting using force vector fields: the part reaches unique orientation after two squeezes. Such orientating strategies exist for all polygonal parts. (The yellow arrows represent the force vector in the corresponding area of the plane; they are *not* arrow-shaped actuators.) See http://www.cs.cornell.edu/home/karl/MicroManipulation for an animated simulation.
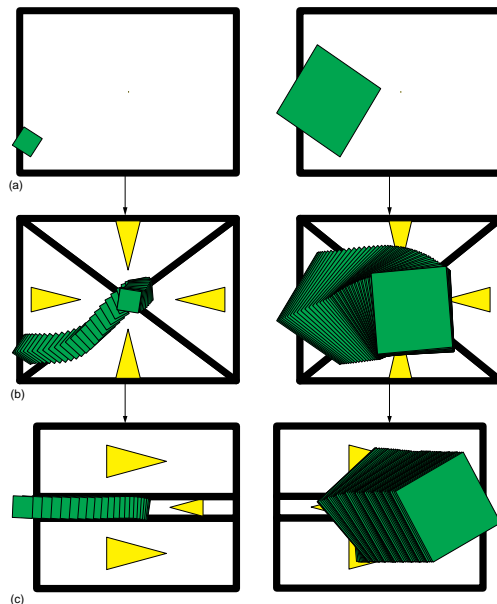

Figure 2. Sensorless sorting using force vector fields: parts of different sizes are first centered and then separated depending on their size.

manipulation strategies and effective actuator arrays may be developed.

We are interested in the algorithmic content of MEMS control strategies, and show how to quantify it, by analyzing the complexity of (1) computing a manipulation plan, (2) the generated plans (that is, force field sequences), and (3) the individual fields. We give upper and lower complexity bounds on plans and fields, and find trade-offs between these different kinds of complexity. We solve the problems of planning and control of microactuator arrays for a wide range of tasks, and present algorithms that automatically generate manipulation plans for translating, orienting, centering, and sorting of small parts (see, for example, Figures 1 and 2).

Equilibria and potentials

When a part is placed on the array, the programmed vector field induces a force and moment upon it. Over time, the part may come to rest in a dynamic equilibrium state. By chaining together sequences of vector fields, the equilibrium states of a part in the field may be cascaded to obtain a desired final state—for example, this state may represent a unique orientation or pose of the part (see Figure 1). The resulting strategies work from any initial configuration (pose) of the part, require no sensing, and enjoy efficient planning algorithms. A system with such a behavior exhibits the *feeding property*[3]:

> A system has the *feeding property* over a set of parts $\mathcal{P}$ and a set of initial configurations $\mathcal{I}$ if, given any part $P \in \mathcal{P}$, there is some output configuration $\mathbf{q}$ such that the system can move P to $\mathbf{q}$ from any location in $\mathcal{I}$.

In the last section of this article we present several force vector fields that possess the feeding property. Some of these fields are more powerful part feeders, as they allow the choice of a specific output configuration $\mathbf{q}$. Our work on programmable vector fields is related to nonprehensile manipulation[4-6]: in both cases, parts are manipulated without form or force closure.

Even though our fields are typically not smooth, it is possible to define a *potential* for certain fields (as a unique path integral). Vector fields with potential have been shown to be theoretically well-suited for manipulation strategies, by classifying a subfamily of potential fields in which every part has stable equilibria. Hence, such fields have been proposed for manipulation tasks in which we desire to cascade equilibria in order to uniquely pose or orient a part (for details see elsewhere[1,2]). The theory of program-

mable vector fields permits calculation of stable equilibria for macroscopic parts in potential fields. (While this question has been well-studied for a point mass in a field, the issue is more subtle when lifted to a body with finite area, due to the moment covector. See elsewhere[1] for details.) In our experiments, we employed vector fields with potential for parts-orientation and parts-posing tasks, and the theory was used to predict the equilibrium poses of specific parts. The poses predicted by the equilibrium analysis were observed in our experiments, as shown in figures we will present in the section "High-Level Control: Vector Fields."

Perhaps surprisingly, the theory also predicts the existence of pathological fields that do not induce well-behaved equilibria. In particular, there exist perfectly plausible vector fields which induce *no* stable equilibrium in very simple parts. Although these fields are very simple, they result in limit cycles and quite complex behavior. We implemented such fields on an array of microcilia, as we discuss later. Vector fields *without* potential were employed to cast parts into limit cycles, such as "infinite" rotation using a skew-symmetric squeeze field. The predicted behavior for such "unstable" vector fields was also observed, as we will illustrate. This shows that rather complex—but potentially useful—behavior can be generated using very simple fields.

We report on our experiments in implementing this theory using microfabricated actuator arrays. Strategies were programmed in a fine-grained SIMD (single instruction, multiple data) fashion by specifying planar force vector fields. These programmable fields were implemented by moving the individual actuators in a cyclic, gaitlike fashion. Motion in nonprincipal (for instance, diagonal) directions was effected by a pairwise coupling of the actuators to implement *virtual actuators* and *virtual gaits* (analogous to the virtual legs employed by Raibert's hopping and running robots[7]). The tasks of translation, rotation, orientation, and centering of parts were demonstrated using small integrated circuit dies. Moreover, the theory of programmable vector fields and virtual gaits gives a method for controlling a very large number of distributed actuators in a principled, geometric, task-level fashion. Whereas many control theories for multiple independent actuators break down as the number of actuators becomes very large, our systems will only become more robust as the actuators become denser and more numerous.
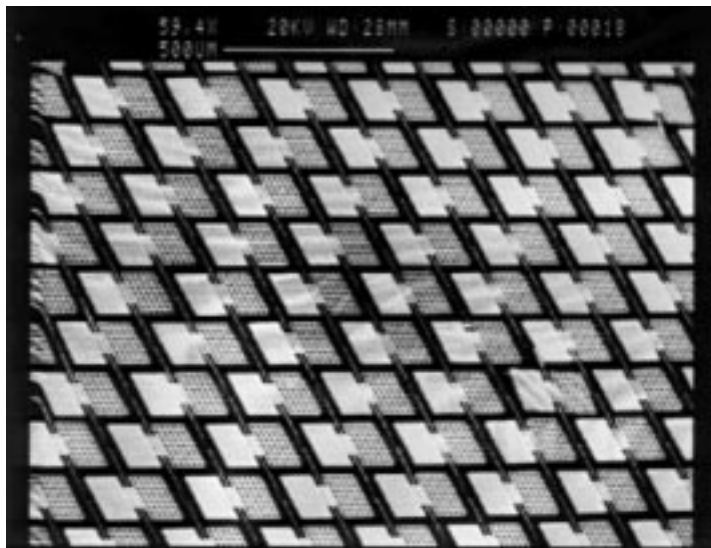

Figure 3. Prototype M-Chip: scanning electron micrograph of a large unidirectional actuator array. Each actuator is 180 μm $\times$ 240 μm in area. Detail from a 1-inch-square array with more than 11,000 actuators. For more pictures on device design and fabrication see http://www.cs.cornell.edu/home/karl/MicroActuators.

Experimental devices and setup

Several groups have described efforts to apply MEMS actuators to positioning, inspection, and assembly tasks with small parts.[2,8–11] However, the fabrication, control, and programming of microdevices that can interact and actively change their environment remains challenging. Problems arise from

♦ the limited range of motion and force that can be generated with microactuators,
♦ the lack of sufficient sensor information with regard to manipulation tasks,
♦ design limitations and geometric tolerances due to the fabrication process, and
♦ uncertain material properties and the lack of adequate models for mechanisms at very small scales.

The following subsections describe two types of actuator arrays that we used: single-crystal silicon electrostatic actuators, and microcilia arrays made of polyimide whose operation is based on combined thermobimorph and electrostatic function.

Single-crystal silicon electrostatic actuators

The M-Chip (manipulation chip, see Figure 3) is fabricated using a Scream (single-crystal silicon reactive etching and metallization) process developed in the Cornell Nanofabrication Facility.[12,13] The Scream process is low-
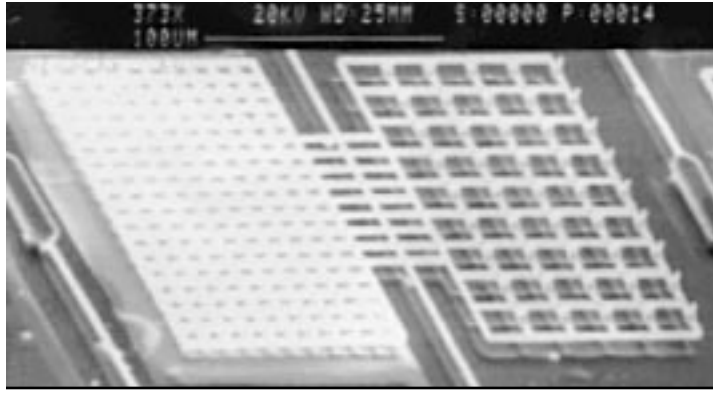
Figure 4. Scanning electron micrograph of a released asymmetric actuator for the M-Chip. *Left:* dense grid (10-μm spacing) with aluminum electrode underneath. *Right:* grid with 5-μm-high poles.
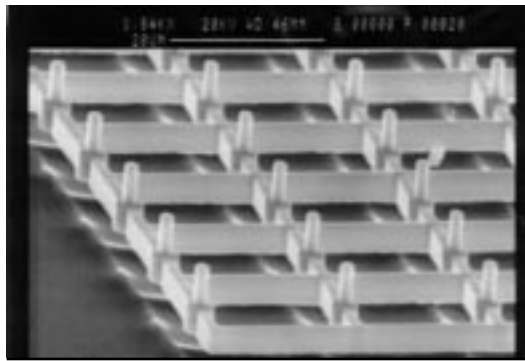

Figure 5. Released M-Chip actuator consisting of single-crystal silicon with 5-μm-high tips, suspended 5 μm above the silicon substrate.
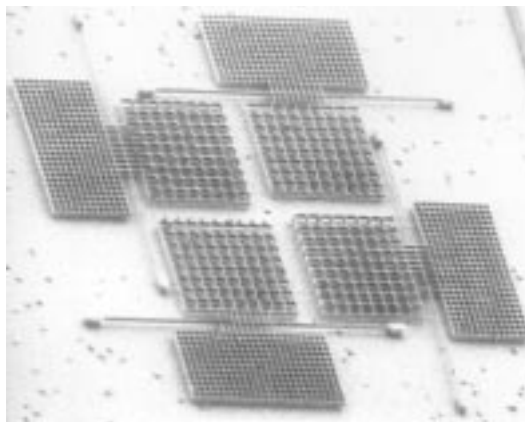

Figure 6. M-Chip prototype motion pixel consisting of actuators oriented in four different directions.

temperature, and does not interfere with traditional VLSI.[14] Hence it opens the door to building monolithic microelectromechanical systems with integrated microactuators and control circuitry on the same wafer.

The design is based on microfabricated torsional resonators.[15,16] Each unit device consists of a rectangular grid etched out of single-crystal silicon suspended by two rods that act as torsional springs (Figure 4). The grid is about 200 μm long and extends 120 μm on each side of the rod. The rods are 150 μm long. The current asymmetric design has 5-μm-high protruding tips on one side of the grid that make contact with an object lying on top of the actuator (Figure 5). The other side of the actuator consists of a denser grid above an aluminum electrode. If a voltage is applied between silicon substrate and electrode, the dense grid above the electrode is pulled downward by the resulting electrostatic force. Simultaneously the other side of the device (with the tips) is deflected out of the plane by several μm. Hence an object can be lifted and pushed sideways by the actuator.

Because of its low inertia (resonance in the high kHz range) the M-Chip can be driven in a wide frequency range from dc to several hundred kHz ac. The actuators need not be operated at resonance: they can also be servoed to periodically "hit" an object on top, hence applying both lateral and vertical forces. Calculations, simulations, and experiments have shown that the force generated with a torsional actuator is approximately 10 μN, which corresponds to a force-per-area ratio of 100 μN/mm^2, large enough to levitate, for example, a piece of paper (1 μN/mm^2) or a silicon wafer (10 μN/mm^2).

Each actuator can generate motion in one specific direction if it is activated; otherwise it acts as a passive frictional contact. Figure 3 shows a small section of a unidirectional actuator array, which consists of more than 11,000 individual actuators. The combination and selective activation of several actuators with different motion bias allows us to generate various motions in discrete directions, spanning the plane (Figure 6). In initial manipulation experiments, small pieces of glass (size several mm^2, mass about 1 mg) were lifted within the motion range of the actuators (several μm) and pushed sideways by several hundred μm.

The fabrication process and mechanism analysis are described in more detail elsewhere.[2,17,18]

Cilia arrays combining thermobimorph and electrostatic actuation

Surface micromachining techniques were used to create microcilia arrays (Figure 7), consisting of polyimide as the primary structural material and aluminum as a sacrificial layer. The fabrica-

tion process (developed at the Center for Integrated Systems, Stanford University) was designed to be compatible with CMOS or BiCMOS circuits which could be prefabricated on a silicon substrate.[19]

Actuator cilia. Each thermobimorph cilium consists of two layers of polyimide with different thermal expansion coefficients. The cilium also contains a titanium-tungsten (Ti:W) resistive heater loop for thermal actuation, aluminum electrodes for electrostatic (low-power) hold-down, and a silicon nitride encapsulation/stiffening layer (Figure 8). For a detailed description of the fabrication process see elsewhere.[19] The cilium is "up" when it is *off*, and is held down to the substrate when on; manipulation is effected by turning the cilium off so that it rises from the held-down position and comes in contact with a part riding atop the cilia array. Vertical and horizontal displacements (δ_v and δ_h) of the cilia tips are a function of the thermal mismatch (thermobimorphism) in the actuator layers. For room temperature, these values can be calculated as $\delta_v \approx 120\ \mu m$ and $\delta_h \approx 20\ \mu m$.[19] Inspection under the scanning electron microscope (SEM) has verified these calculations.

The cilia array is composed of cells or "motion pixels," each 1.1 mm square, which contain four orthogonally oriented actuators, each of which is a little less than half a millimeter long (Figure 9). The lifting capacity of a single actuator can be estimated as the force required to deflect the actuator's tip to the substrate. The actuator load capacity has been calculated as $F_l = 76\ \mu N$, which gives a force-per-area ratio of $4 \times 76\ \mu N/(1.1\ mm)^2 \approx 250\ \mu N/mm^2$.

Chip layout. On the current cilia chip, the motion pixels are arranged in an 8×8 array which occupies approximately $0.77\ cm^2$ of a 1-cm^2 die (see Figure 7). The four actuators of each pixel are independently activated by four thermal and four electrostatic control lines.
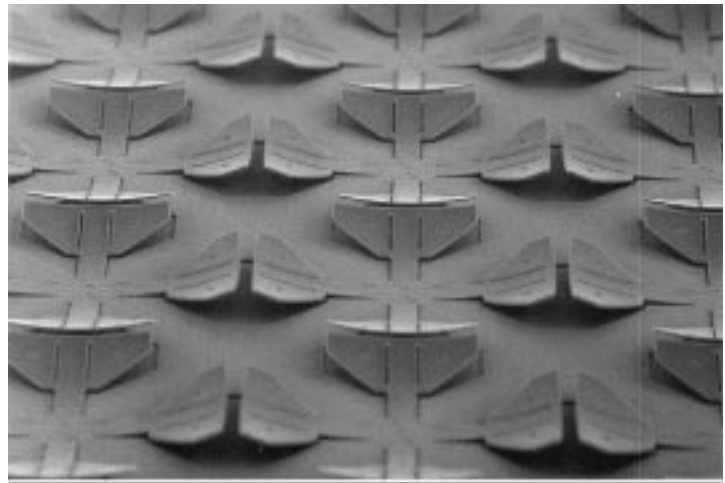

Figure 7. Portion of a polyimide cilia array (SEM micrograph). Four orthogonally oriented actuators are integrated into a "motion pixel," each of which covers a surface area approximately 1.1 mm square.
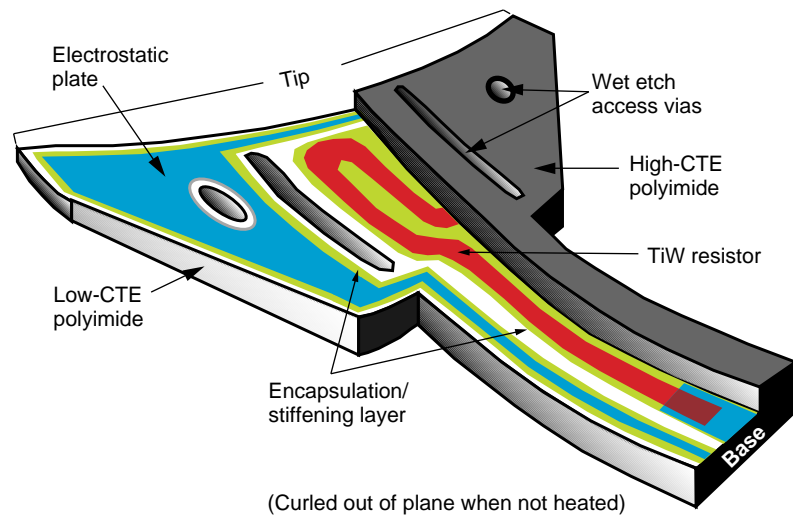

Figure 8. Thermal and electrostatic microactuator. Half of the upper polyimide and silicon nitride encapsulation/stiffening layer is cut away along the cilium's axis of symmetry to show details.
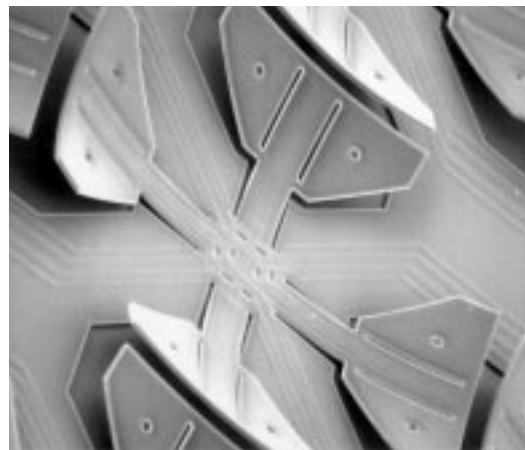

Figure 9. Polyimide cilia "motion pixel" (SEM micrograph). Four actuators in a common-center configuration make up a motion pixel. Each cilium is 430 μm long and bends up to 120 μm out of the plane.
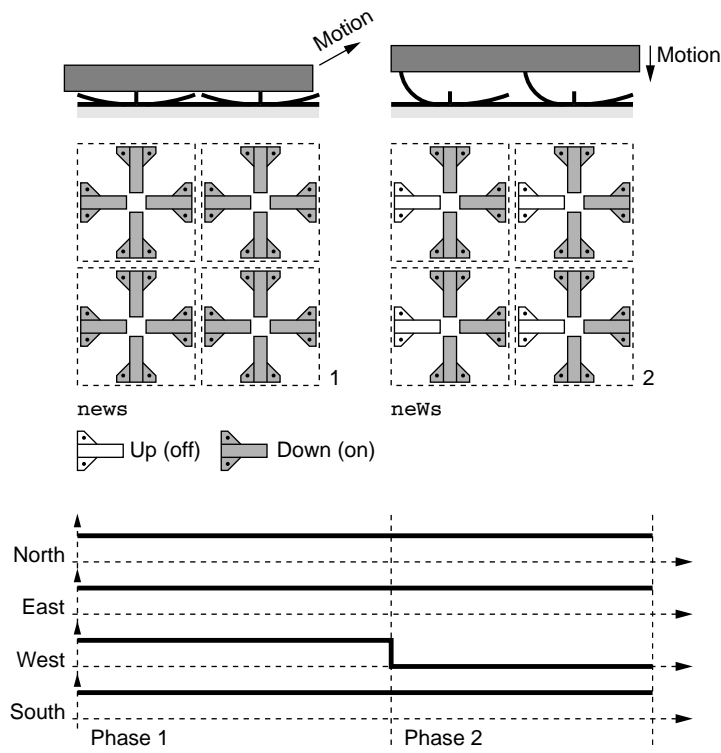
Figure 10. Two-phase gait. The **w** actuator is repeatedly switched on and off, while the other actuators always remain on, resulting in a **news neWs** sequence. (Squares show the top view. Above the top view of each numbered phase, an edge view shows how the cilia make contact with a part moving over the array.)

Four 8×8 chips are diced and packaged together to make a quad-shaped 16×16–pixel cilia array device, with a total of 1,024 cilia. The device itself is attached to a hybrid package which is placed on a heat sink and thermoelectric cooler (Peltier-effect module). The total input power to the chip can exceed 4 W, and without active cooling the package can become very hot. To observe the experiments, a long-working-distance microscope is connected to a CCD camera, and a videocassette recorder is used to monitor and record both the movements of an individual cilium and the objects conveyed by the array.

Controller. The manipulation results described below were accomplished with the cilia array device interfaced to an IBM 486 personal computer. The PC provides speed control via the drive pulse frequency and directional control interactively via keyboard or mouse, or by actuator programs that can be specified using the MEMSA (MEMS array) language which we developed at Stanford. (MEMSA, named after the Mensa organization, is a language for smart

manipulation surfaces.) The control software, including the MEMSA interpreter, was written in Pascal. Thermal and electrostatic control line signals are sent via the PC parallel port to D-type flip-flops which activate power transistors. Currently up to four cilia arrays can be controlled simultaneously by using a multiplexer with two address bits.

In the remainder of this article we will concentrate on the operation of the microcilia arrays for various manipulation tasks.

Low-level control: Actuator gaits

To induce motion on a part that is placed on the array, the cilia are actuated in a cyclic, gaitlike fashion. In each cycle, the part is moved in a certain direction by the motion of the actuators that are in contact with it. The speed of the moving part depends on the (horizontal) displacement of the actuators per cycle as well as the frequency of cycle repetition. It also depends on the surface properties and weight of the moving part.

Task: translation of parts in principal directions

The simplest gait is the *two-phase gait*, in which all actuators (cilia) of one orientation repeatedly stroke the part while the remaining actuators are held down. Assuming that the orthogonal cilia within a motion pixel are oriented at the principal compass points, let us use capital letters **NEWS** to denote the North, East, West, and South actuators in the up position, and lowercase letters **news** to denote the actuators in the lowered position. Then the two-phase gait to effect motion in the East direction would be **news neWs** (see Figure 10).

The *four-phase gait* consists of four different actuation phases **news neWs nEWs nEws** such that motion is induced during upward as well as downward strokes of the cilia (Figure 11, see elsewhere also[9]). Note that the forces exerted on the moving part depend on the state of the motion pixel. For example, in the transition from Phase 1 to Phase 2 the cilium **W** moves up while the opposing cilium **e** remains down. We denote the lateral force exerted on the part in this configuration $f_{W,e}$. (Here, where just two directions are relevant, the first index denotes the active cilium, showing its state after the action. The second index is the cilium that did not move.) Analogously, during transitions 2–3, 3–4, and 4–1 we observe lateral forces $f_{E,W}$, $f_{w,E}$, and $f_{e,w}$, respectively. The forces $f_{W,e}$ and $f_{e,w}$ are in the positive x-direction, while $f_{E,W}$ and $f_{w,E}$ are
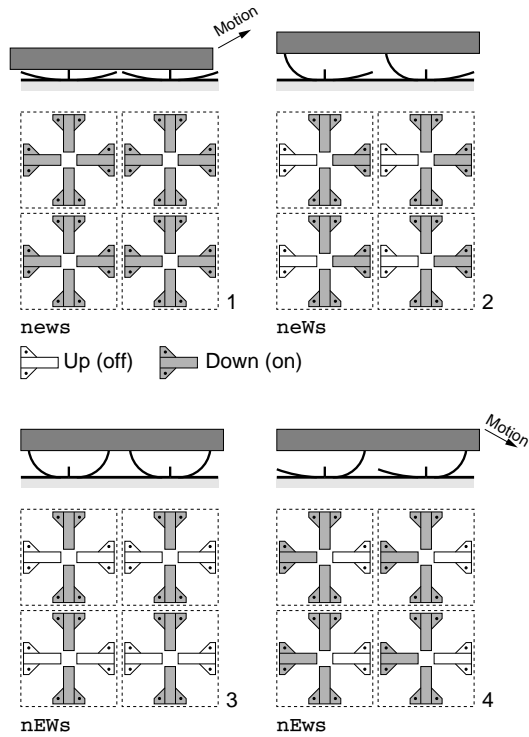
Figure 11. Four-phase gait consisting of the four-pattern sequence `news neWs nEWs nEws`.

hopping and running robots.[7] Hence, several cilia can be coordinated to emulate a virtual cilium, which generates a force corresponding to the vector sum of its components. The diagonal gait to effect motion in the Northeast direction would be `news neWS NEWS NEws`, where the virtual cilia are `NE` and `WS` (see Figure 12). Consequently, we obtain a *virtual gait* that moves the part in a diagonal direction. Note that in a section view through the array looking in the Northwest direction, this gait would look virtually identical to the four-phase gait depicted in Figure 11.

Motion in arbitrary directions can be induced by alternating gaits that interleave principal (or virtual) gaits of different directions. For example, a translation at 25° from the *x*-axis requires motion in the *y*-direction and *x*-direction at a ratio of tan 25° ≈ 1:2. Our control software determines the exact alternation analogously to the Bresenham line scan algorithm,[20] which rasterizes lines at arbitrary angles, resulting in different fields that are interlaced in time.
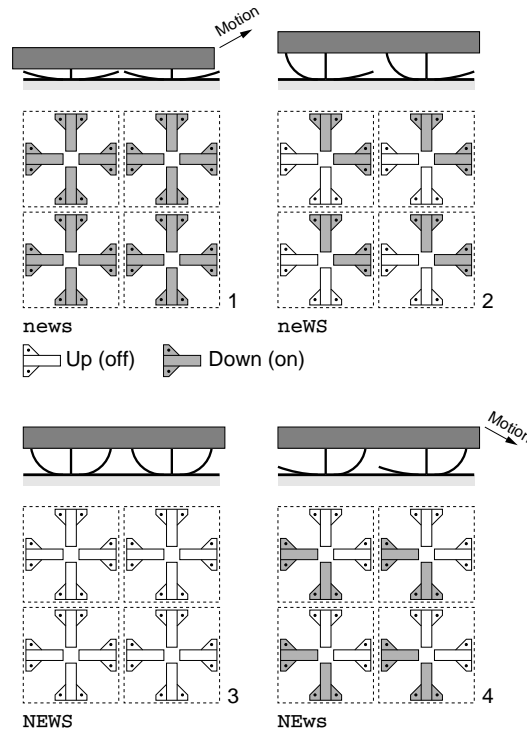
negative. Furthermore, from Figure 11 we conclude that $f_{W,e}$ and also $f_{e,w}$ generate stronger forces on the part, while $f_{E,W}$ and $f_{w,E}$ are negligible. This is because in transitions 2–3 and 3–4, the great majority of the time the active cilia are moving they are not in contact with the part. Specifically,

$$\left| f_{W,e} \right| \gg \left| f_{e,w} \right| \gg \left| f_{E,W} \right| \approx \left| f_{w,E} \right| \approx 0.$$

Hence we expect a relatively large motion step $\Delta x_{W,e}$ during transition 1–2, and a smaller step $\Delta x_{e,w}$ during transition 4–1, while during the other transitions the part remains at its current location. We have observed this behavior in our physical experiments, where $\Delta x_{W,e}$ was measured at between 3 μm and 10 μm depending on input power, frequency, surface properties, and weight of the part. The motion $\Delta x_{W,e}$ was usually about twice as large as $\Delta x_{e,w}$.

Task: Translation of parts in arbitrary directions

Motion in nonprincipal (such as diagonal) directions is effected by a pairwise coupling of two cilia of each pixel, implementing *virtual cilia* analogous to Raibert's concept of virtual legs for

Figure 12. Diagonal (virtual) gait consisting of the four-pattern sequence `news neWS NEWS NEws`. The `N` and `E` cilia, and the `W` and `S` cilia, are coupled to form virtual cilia in Northeast and Southwest directions. (Sectional view here is looking in the North direction.)
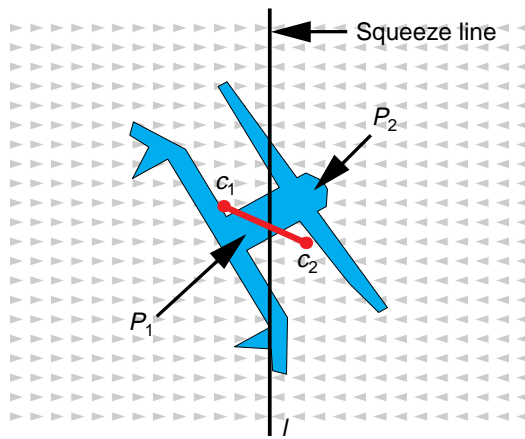
Figure 13. Equilibrium condition: to balance force and moment acting on P in a unit squeeze field, the two areas P_1 and P_2 must be equal (that is, l must bisect the part), and the line connecting the centers of areas c_1 and c_2 must be perpendicular to the squeeze line l.

Experiments and results

We have performed a large number of translation experiments in which two-phase and four-phase gaits were used to implement principal and virtual gaits. These experiments show that a first-order dynamical system models the device–part interaction well. Therefore, when describing and predicting the motion of parts in force vector fields, we have based our theory on a first-order system (see the section on High-Level Control).

Silicon chips were moved with a motion resolution of a few μm and speeds up to 200 μm per second. Four-phase gaits proved more effective than two-phase gaits, because during the downward motion in the two-phase gait, the part tends to slip backwards. The four-phase gait avoids this effect, because other cilia hold the part in place during the transition 3–4. In the subsequent downward motion in the transition 4–1, the part is also moved forward (Figure 11).

The diagonal gait also has the lowest power consumption (not considering electrostatic hold-down), due to the fact that its duty cycle for cilia hold-down is lowest (50 percent), compared to 75 percent for the principal four-phase gait, and 87.5 percent for the two-phase gait.

As expected, diagonal (virtual) gaits induced the largest and fastest motion because all four cilia of each pixel were activated, whereas in principal gaits only two cilia are actively used, while the others have to be held down continuously (Figure 11).

High-level control: Vector fields

We believe that vector fields can be used as an *abstraction barrier* between applications requiring array micromanipulation and MEMS devices implementing the requisite mechanical forces. That is, applications such as parts-feeding can be formulated in terms of the vector fields required. This then serves as a specification which the underlying MEMS device technology must deliver. Conversely, the capabilities of MEMS array technologies for actuation can be formulated in terms of the vector fields they can implement. For example, limitations in force magnitude are naturally expressed in vector field terms, as "small" vector fields. Restrictions in directional selectivity and magnitude control can also be manifested as restrictions on the vector field abstraction (resulting in discretization in orientation or modulus).

This means that designers of MEMS actuator arrays could potentially ignore certain details of the application process, and instead focus on matching the required vector field specification. Then, once the capabilities of MEMS actuator arrays were published as vector fields and tolerances, an application designer could look in a catalog to choose a device technology based on the field specification it promises to implement. This would free application engineers from needing to know much about process engineering, in the same way that software and algorithm designers often abstract away from details of the hardware. Such an abstraction barrier could permit hierarchical design, and allow application designs with greater independence from the underlying device technology. At the same time, abstraction barriers could allow MEMS array technologies to be designed simultaneously with the (abstract) vector field control. This development pattern could be similar to the concurrent design of VLSI processors with their compilers, as is common in computer architecture.

Squeeze fields

A previous article[2] proposed a family of control strategies called *squeeze fields* and a planning algorithm for parts orientation (see Figures 1 and 13).

Definition 1. Given a straight line l, a squeeze field *f is a two-dimensional force vector field in which, at each point, a unit force points perpendicularly towards l (on l the force is zero).*[1]

We refer to the line l as the *squeeze line*, because l lies in the center of the squeeze field. Assuming quasi-static motion, an object will translate and rotate to an equilibrium configuration,

as characterized in Figure 13. To predict the equilibria, we assume a uniform force distribution over the surface of *P*, which is a reasonable assumption for a flat part that is in contact with a large number of elastic actuators.

Definition 2. A part P is in translational equilibrium *if the forces acting on P are balanced. P is in* orientational equilibrium *if the moments acting on P are balanced.* Total equilibrium *is simultaneous translational and orientational equilibrium.*

Claim 3.[1] *Every squeeze field f (see Definition 1) has potential, of the form*

$$U(\mathbf{z}) = \int_\alpha f \cdot ds,$$

where α is an arbitrary path to $\mathbf{z}$ from a fixed reference point. If $d_\mathbf{z}$ denotes the perpendicular distance of $\mathbf{z}$ from the squeeze line, then $U(d_\mathbf{z}) = |d_\mathbf{z}|$.

Claim 4.[1] *Let P be a connected polygonal part with finite contact area and n vertices. Then in any squeeze field, P has $E = O(kn^2)$ orientation equilibria, where k is the maximum number of edges that a bisector of P can cross. If P is convex, then the number of equilibria is O(n).*

Equilibria can be calculated numerically using the method in Figure 13: Given an arbitrary part at a fixed orientation, we translate it until its left and right sections have equal size. If the respective centers of gravity lie on a line perpendicular to the squeeze line, then the part is in equilibrium. For polygonal parts there exist analytical methods to compute the equilibria exactly (see elsewhere[1] for a detailed algorithm and a derivation of the $O(kn^2)$ bound).

Claim 5. Let P be a polygon whose interior is connected. There exists a sensorless alignment strategy consisting of a sequence of squeeze fields that uniquely orients P up to symmetries in part and field geometry.[1]

Proof of Claim 5. Claim 4 states that a squeeze field brings a polygon *P* into one of $E = O(kn^2)$ orientation equilibria. We define the *squeeze function* as this mapping from original orientation to equilibrium orientation. Hence, from Claim 4 it follows that the image of the squeeze function is a set of *E* discrete values. Given such a squeeze function, Goldberg has presented an algorithm for sensorless manipulation of polygons[21] that constructs an orienting strategy with $O(E)$ steps in $O(E^2)$ time. The output of this algorithm is a sequence of squeeze directions. When the corresponding squeeze fields are applied to the part *P*, the set of possible orientations is successively reduced until a unique orientation (up to symmetry) is reached. For details see elsewhere.[1,21]

Task: orienting and aligning parts. If a part is placed in a squeeze field, it will translate and rotate until a stable equilibrium is reached (Claim 4). Parts may exhibit several equilibria, hence after one squeeze the part orientation may be ambiguous. This ambiguity can be removed with the strategies of Claim 5: by executing a sequence of squeezes at particular angles, the part is uniquely oriented (refer back to Figure 1).

Experiments and results. The oblong trapezoidal part depicted in Figure 14 (left side) and
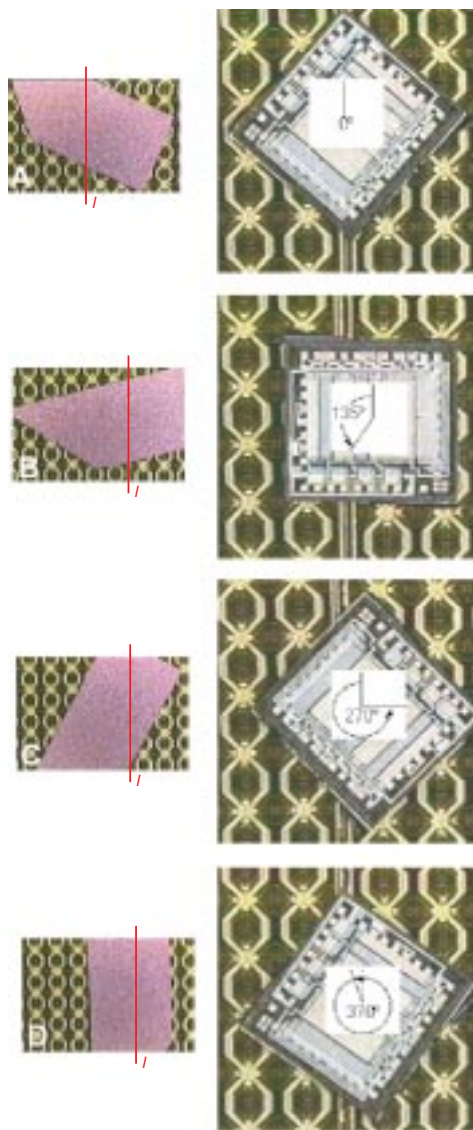

Figure 14. Manipulation of silicon chips in programmable vector fields induced by a microcilia array (microscope video images). *Left:* the chip is aligned with the vertical squeeze line *l* (marked by a dark line for clarity). *Right:* rotating a square-shaped chip counterclockwise in a skewed squeeze field.
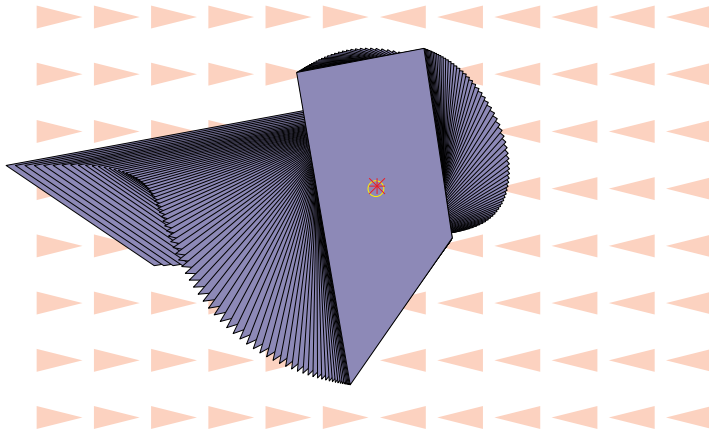
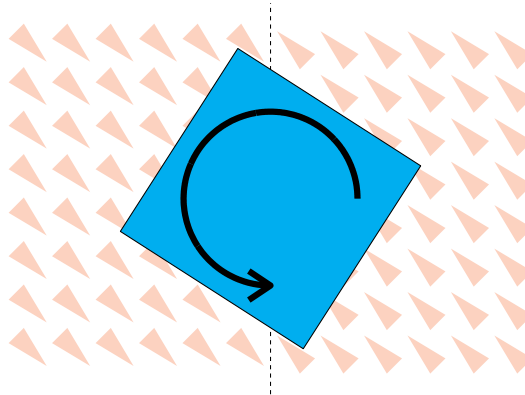Figure 15. Simulation of the alignment task with a squeeze field as shown in the left side of Figure 14.

Figure 16. Unstable square-shaped part in a skewed squeeze field ($\varepsilon = -1$). The square with center on the squeeze line will rotate indefinitely. Moreover, it has no stable equilibrium in this field.

Figure 15 exhibits a unique stable equilibrium (modulo 180° field symmetry). When placed in a squeeze field, its longitudinal axis aligns with the squeeze line. This dynamic process is predicted by simulation in Figure 15, and verified in experiment (see left side of Figure 14). This part alignment experiment has also been performed with similar results for several other small pieces of glass and silicon of a few mm length and several mg of mass.

Skewed squeeze fields

A variation on the squeeze field is the *skewed* squeeze field.

Definition 6.[1] *A skewed field f_S is a vector field given by $f_S(x, y) = -\text{sign}(x)(1, \varepsilon)$, where $0 \neq \varepsilon \in \mathbb{R}$.*

(The value ε is the skew factor, or the degree of skewedness of the skewed field.)

Claim 7.[1] *No skewed squeeze field has a potential.*

In a skewed squeeze field, it is easy to find a circular path along which the work integral is nonzero (for example, along a circle with its center on the squeeze line).

Claim 8.[1] *A skewed field induces* no *stable equilibrium on a disk-shaped part (for all $\varepsilon \neq 0$).*

Force equilibrium is only possible if the center of the disk coincides with the squeeze line. In this position the disk experiences a nonzero moment if $\varepsilon \neq 0$.

Claim 9.[1] *A diagonally skewed field ($\varepsilon = \pm 1$) induces* no *stable equilibrium on a square-shaped part.*

For a proof see Ref. 1.

Task: rotating parts. According to Claims 8 and 9, certain parts will rotate indefinitely in skewed squeeze fields (Figure 16). Note that even though our cilia device has more degrees of freedom, two areas of constant force are sufficient to implement a skewed field, resulting in a very simple task-level rotation strategy. In particular, the rotation algorithm resulting from the application of skew-symmetric squeeze fields is considerably simpler than rotation algorithms proposed in the MEMS literature (for example, the vortices suggested by Fujita[10] or by Liu and Will[11]). Vortices require at least four areas of the array to be pushing in different directions. That is, vortices can be implemented using four triangular or rectangular regions, upon each of which the vector field is constant. Skewed fields perform the same task with only two regions of constant force.

Experiments and results. The right side of Figure 14 shows video frames of a 3 mm × 3 mm IC chip rotating on the squeeze line of a skewed field. During experiments lasting approximately 10 minutes, several full rotations of the part were performed.

Radial fields

The third kind of vector field we will consider is the radial field.

Definition 10. A radial field f is a two-dimensional force vector field such that $f(\mathbf{z}) = -\mathbf{z}/|\mathbf{z}|$ if $\mathbf{z} \neq 0$, and $f(\mathbf{0}) = \mathbf{0}$.

Claim 11.[1] *A radial field has a potential, $U(\mathbf{z}) = |\mathbf{z}|$.*

Claim 12.[1] *Given a polygonal part P in a radial field f, there exists a unique pivot point v of P such that P is in equilibrium if and only if v coincides with the center of the radial field.*

Claim 13.[1] *Let P be a polygonal part with n vertices, and let k be the maximum number of edges*

Table 1. Summary of manipulation tasks.

| Task | Field(s) | Complexity | | |
		Fields	Planning	Plan steps
Translate	Constant	Constant magnitude and direction	—	1
Center	Radial	Constant magnitude, continuous directions	—	1
Uniquely orient	Sequence of squeezes	Piecewise constant magnitude and direction	$O(k^2n^4)$	$O(kn^2)$
	Inertial	Smooth magnitude, piecewise constant direction	$O(1)$	$O(1)$
Uniquely pose	Sequence of radial + squeeze	Piecewise continuous magnitude and direction	$O(k^2n^2)$	$O(kn)$
	Elliptic	Smooth magnitude and direction	$O(1)$	$O(1)$
	UFO	Continuous magnitude and direction	—	1

that a bisector of P can cross. There are at most $E = O(kn)$ stable equilibria in a field of the form $R + \delta S$ if S is a squeeze field, and δ is sufficiently small and positive.

Proofs of the previous claims, and a numerical algorithm to compute the pivot point, are given elsewhere.[1] Note that Claim 13 results in strategies for unique parts posing in $O(E) = O(kn)$ steps.

Task: centering parts. Radial fields can be used to center a part. With the current four-quadrant cilia device, we have implemented an approximation of an ideal radial field similar to the field in Figure 2b. Note that this approximate radial field has a potential.

Experiments and results. We centered small silicon and glass parts using our cilia device. In this experiment, high positioning accuracy (in the μm range) was hard to achieve, because the center of the radial field coincides with the location of the interior edges of the dies that make up the cilia array. Manual packaging of the four cilia chips leaves small gaps and nonplanarities at these junctions. The next-generation cilia device will overcome this problem, because it will allow us to implement the radial field with a single chip. Furthermore, because of its full pixelwise programmability, the new chip will allow us to closely approximate ideal radial fields.

Table 1 summarizes fields and algorithms for manipulation tasks with programmable vector fields, and includes some additional recent results.

Less difficult tasks such as translation can be achieved with relatively simple fields and without any planning. More complex tasks such as centering or unique orienting require increasingly complex fields. However, planning complexity is, for example, higher for sequences of squeeze fields, and lower for the more complex combined radial plus squeeze fields (for a thorough discussion of these fields see elsewhere[1]). This illustrates a trade-off between mechanical complexity (the dexterity and controllability of actuator array elements) and computational complexity (the algorithmic difficulty of synthesizing a strategy).

Our research leads to the question about the existence of a "universal feeder-orienter" (UFO) device that uniquely poses a part without the need of a clock, sensors, or programming.[22] Kavraki[23] has provided a step in that direction, by presenting an "elliptic" force field $f(x, y) = (\alpha x, \beta y)$ with $\alpha \neq \beta$ and $\alpha, \beta \neq 0$, for which most parts have exactly two total equilibria. An "inertial" squeeze field $f(x, y) = (-\text{sign}(x)x^2, 0)$ uniquely orients a part modulo field symmetry. In a stable equilibrium, the part's major principal axis of inertia lines up with the squeeze line to minimize the second moment of inertia.[22]

We have proposed a combined radial plus "gravitational" field $R + \delta G$ which might have the UFO property.[1] Such a field could be obtained from a tilted MEMS array that implements a radial field. Extensive simulations show that for every part we have tried, one unique total equilibrium is always obtained. We are working toward a rigorous proof of this experimental observation. ♦

References

1. K.-F. Böhringer, B.R. Donald, and N.C. MacDonald, "Upper and Lower Bounds for Programmable Vector Fields with Applications to MEMS and Vibratory Plate Parts Feeders," in *Algorithms for Robotic Motion and Manipulation,* J.-P. Laumond and M. Overmars, eds., A.K. Peters, Wellesley, Mass., 1997, pp. 255–276. Also at http://www.cs.cornell.edu/home/karl/MicroManipulation.

2. K.-F. Böhringer et al., "A Theory of Manipulation and Control for Microfabricated Actuator Arrays," *Proc. IEEE Workshop on Micro Electro Mechanical Systems (MEMS)* [Oiso, Japan], Jan. 1994, pp. 102–107. Also at http://www.cs.cornell.edu/home/karl/MicroActuators.

3. S. Akella et al., "Planar Manipulation on a Conveyor by a One Joint Robot With and Without Sensing," *Proc. Int'l Symp. Robotics Research (ISRR),* 1995.

4. B.R. Donald, J. Jennings, and D. Rus, "Information Invariants for Distributed Manipulation," in K. Goldberg et al., eds., *Algorithmic Foundations of Robotics,* A.K. Peters, Wellesley, Mass., 1995, pp. 431–459.

5. N.B. Zumel and M.A. Erdmann, "Nonprehensile Two Palm Manipulation with Non-Equilibrium Transitions Between Stable States," *Proc. IEEE Int'l Conf. Robotics and Automation (ICRA)* [Minneapolis, Minn.], Apr. 1996.

6. M.A. Erdmann, *An Exploration of Nonprehensile Two-Palm Manipulation: Planning and Execution,* Tech. Report, Carnegie Mellon Univ., Pittsburgh, Pa., 1996.

7. M.H. Raibert et al., "Animation of Legged Maneuvers: Jumps, Somersaults, and Gait Transitions," *J. Robotics Soc. of Japan,* Vol. 11, No. 3, 1993, pp. 333–341.

8. K.S.J. Pister, R. Fearing, and R. Howe, "A Planar Air Levitated Electrostatic Actuator System," *Proc. IEEE Workshop on Micro Electro Mechanical Systems (MEMS)* [Napa Valley, Calif.], Feb. 1990, pp. 67–71.

9. M. Ataka, A. Omodaka, and H. Fujita, "A Biomimetic Micro Motion System," *Transducers: Digest Int'l Conf. on Solid-State Sensors and Actuators* [Pacifico, Yokohama, Japan], June 1993, pp. 38–41.

10. H. Fujita, "Group Work of Microactuators," *Int'l Advanced Robot Program Workshop on Micromachine Technologies and Systems* [Tokyo, Japan], Oct. 1993, pp. 24–31.

11. W. Liu and P. Will, "Parts Manipulation on an Intelligent Motion Surface," *Proc. IROS '95, IEEE/RSJ Int'l Conf. Intelligent Robots and Systems,* IEEE Computer Soc. Press, Los Alamitos, Calif., Vol. 3, 1995, pp. 399–404.

12. Z.L. Zhang and N.C. MacDonald, "An RIE Process for Submicron, Silicon Electromechanical Structures," *J. Micromechanics and Microengineering,* Vol. 2, No. 1, Mar. 1992, pp. 31–38.

13. K.A. Shaw, Z.L. Zhang, and N.C. MacDonald, "SCREAM I: A Single Mask, Single-Crystal Silicon Process for Microelectromechanical Structures," *Transducers: Digest Int'l Conf. on Solid-State Sensors and Actuators* [Pacifico, Yokohama, Japan], June 1993.

14. K.A. Shaw and N.C. MacDonald, "Integrating SCREAM Micromechanical Devices with Integrated Circuits," *Proc. IEEE Workshop on Micro Electro Mechanical Systems (MEMS)* [San Diego, Calif.], Feb. 1996.

15. R.E. Mihailovich et al., "Single-Crystal Silicon Torsional Resonators," *Proc. IEEE Workshop on Micro Electro Mechanical Systems (MEMS)* [Ft. Lauderdale, Fla.], Feb. 1993, pp. 155–160.

16. R.E. Mihailovich and N.C. MacDonald, "Dissipation Measurements of Vacuum-Operated Single-Crystal Silicon Resonators," *Sensors and Actuators,* Part A, Vol. 50, No. 3, 1996, p. 199.

17. K.-F. Böhringer et al., "Sensorless Manipulation using Massively Parallel Microfabricated Actuator Arrays," *Proc. IEEE Int'l Conf. Robotics and Automation (ICRA)* [San Diego, Calif.], May 1994, pp. 826–833. Also at http://www.cs.cornell.edu/home/karl/MicroManipulation.

18. K.-F. Böhringer, B.R. Donald, and N.C. MacDonald, "Single-Crystal Silicon Actuator Arrays for Micro Manipulation Tasks," *Proc. IEEE Workshop on Micro Electro Mechanical Systems (MEMS)* [San Diego, Calif.], Feb. 1996. Also at http://www.cs.cornell.edu/home/karl/MicroActuators.

19. J.W. Suh et al., "Combined Organic Thermal and Electrostatic Omnidirectional Ciliary Microactuator Array for Object Positioning and Inspection," *Proc. Solid State Sensor and Actuator Workshop* [Hilton Head Is., S.C.], June 1996.

20. J.D. Foley et al., *Computer Graphics: Principles and Practice,* 2nd ed., Addison Wesley, 1996.
21. K.Y. Goldberg, "Orienting Polygonal Parts Without Sensing," *Algorithmica,* Vol. 10, Nos. 2/3/4, Aug./Sept./Oct. 1993, pp. 201–225.
22. K.-F. Böhringer, B.R. Donald, and N.C. MacDonald, "Programmable Vector Fields for Distributed Manipulation, with Applications to MEMS Actuator Arrays and Vibratory Parts Feeders," submitted to *Int'l J. Robotics Research,* 1996.
23. L. Kavraki, "Part Orientation with Programmable Vector Fields: Two Stable Equilibria for Most Parts," *Proc. IEEE Int'l Conf. Robotics and Automation (ICRA)* [Albuquerque, N.M.], Apr. 1997.

Karl-Friedrich Böhringer received a Diplom-Informatiker degree from the Technical University of Karlsruhe, Germany, and MS and PhD degrees in computer science from Cornell University, working under Bruce Donald. In his dissertation research he investigated MEMS actuator devices that perform micromanipulation tasks. During his graduate studies, he spent a year with the Robotics and Transducers Laboratories at Stanford University. He recently moved to the University of California, Berkeley, where he performs postdoctoral research on microrobotics and self-assembly. Böhringer and Ken Goldberg codirect the Alpha (assembly line and parts handling) laboratory of the Department of Industrial Engineering and Operations Research at Berkeley.

Bruce R. Donald received an SM in EECS and a PhD in computer science at the Artificial Intelligence Laboratory at MIT, working under Tomas Lozano-Perez. He is cofounder of the Robotics and Vision Laboratory at Cornell University, where he is currently an associate professor in the Department of Computer Science. Donald received a National Science Foundation Presidential Young Investigator award in 1989. He has written three books and numerous scientific papers on robotics; he has also been a visiting professor at Stanford University and has worked at Interval Research Corp. (Palo Alto) to develop precompetitive technologies in graphics and multimedia. E-mail, brd@cs.cornell.edu.

Noel C. MacDonald is professor of electrical engineering at Cornell University and director of the Cornell Nanofabrication Facility. He received his doctorate in electrical engineering (1967) from the University of California at Berkeley. In 1970 he joined Physical Electronics Industries, later acquired by Perkin-Elmer Corp.; he remained in various management posts at Perkin-Elmer until 1983, and then went to Cornell as professor of electrical engineering and director of the Program on Microscience and Technology. In 1989 he became director of Cornell's School of Electrical Engineering. MacDonald has specialized in electron-beam technology, with emphasis on microelectronic applications; he was instrumental in combining Auger electron spectroscopy with scanning electron microscopy and in developing the scanning Auger microprobe. He serves on the Sematech University Advisory Board, the International MEMS Steering Committee, and the advisory board for the International Symposium on Electron, Ion, and Photon Beams. He is a member of IEEE, the American Physical Society, the American Vacuum Society, the Electrochemical Society, and the Materials Research Society. E-mail, nmacd@ee.cornell.edu.

Gregory T.A. Kovacs is assistant professor at the Transducers Laboratory, Department of Electrical Engineering, Stanford University. Kovacs received the BASc degree in electrical engineering from the University of British Columbia, Vancouver, B.C., in 1984, the MS in bioengineering from the University of California, Berkeley, in 1985, the PhD in electrical engineering from Stanford University in 1990, and the MD from Stanford in 1992. He is active in research in the areas of solid-state sensors and actuators, integrated circuit fabrication, micromachining, neuroscience, and biotechnology. Present projects include the development of direct interfaces between external electronics and the nervous systems of various vertebrate animals, biosensors, micromechanical actuators, integration of active signal processing circuitry with micromachined transducers, low-power circuit design for transducer systems, development of robust interconnect technologies for implantable sensors, and investigation of basic transducer technologies. E-mail, kovacs@sensors.stanford.edu.

John W. Suh is a doctoral candidate in mechanical engineering at Stanford University, and works in the Transducers Laboratory of the Stanford Department of Electrical Engineering. He has a BS in electrical engineering from the GMI Engineering and Management Institute (1990) and an MS in mechanical engineering from Stanford University (1992). Earlier he worked in the Mechanical Fabrication Department at the Stanford Linear Accelerator Center, the Stamping Plant Modernization Group of a General Motors division headquarters, and the Transportation Research Department of General Motors Research Laboratories. E-mail, jwsuh@sensors.stanford.edu.

Corresponding author: Karl-Friedrich Böhringer, University of California at Berkeley, Department of Industrial Engineering and Operations Research, 4175 Etcheverry Hall, Berkeley, CA 94720, USA; e-mail, karl@ieor.berkeley.edu.